Neoplasma 2024; 71(4): 347–358

doi:10.4149/neo_2024_240122N35

The role of RRS1 in breast cancer cells metastasis and AEG-1/AKT/c-Myc signaling pathway

Jing HE[1,2,#], Sijing LIU[1,2,#], Shajie LUO[1,2], Jiaojiao FU[1,2], Zhengyue LIAO[1,2], Junying SONG[3], Jinlin GUO[1,2,*], Ya'nan HUA[1,2,3,*]

[1]College of Medical Technology, Chengdu University of Traditional Chinese Medicine, Chengdu, Sichuan, China; [2]Chongqing Key Laboratory of Sichuan-Chongqing Co-construction for Diagnosis and Treatment of Infectious Diseases Integrated Traditional Chinese and Western Medicine, Chengdu, Sichuan, China; [3]Department of Biochemistry and Molecular Biology of Basic Experimental Center Medical College, Medical Department, Qingdao University, Qingdao, Shandong, China

**Correspondence: huayanan@cdutcm.edu.cn; guo596@cdutcm.edu.cn*
#Contributed equally to this work.

Received January 22, 2024 / Accepted June 26, 2024

Breast cancer is the most common malignant tumor in women. Recurrence, metastasis, and chemotherapy resistance are the main causes of death in breast cancer patients. The inhibition of breast cancer metastasis is of great significance for prolonging its survival. Ribosome biogenesis regulatory protein homolog (RRS1) is overexpressed in breast cancer tissues and is involved in regulating the carcinogenic process of breast cancer cells. However, the exact signaling pathway and molecular mechanism of RRS1 promoting breast cancer metastasis are not fully understood. Hence, the primary objective of our study is to investigate the correlation between RRS1 and breast cancer metastasis. Bioinformatic analysis was used to identify the expression levels and prognostic significance of RRS1 in breast cancer. Lenti-sh RRS1 lentivirus was constructed and employed to downregulate the RRS1 expression in MDA-MB-231 and BT549 cells, which had a high-level expression of RRS1. Subsequently, we assessed the impact of RRS1 downregulation on the proliferation, migration, and invasion of breast cancer cells using CCK-8, apoptosis, and cell cycle by flow cytometry, wound healing test, Transwell migration, and invasion experiments. Moreover, we utilized an *in vivo* imaging system to examine the metastatic potential of breast cancer cells after RRS1 knockdown. Picrate staining and hematoxylin-eosin staining were employed to evaluate the presence of metastatic lesions. To gain a deeper understanding of the molecular mechanism, we conducted co-immunoprecipitation and western blot. The significant overexpression of RRS1 in breast cancer indicates a worse prognosis, as determined through TCGA databases ($p<0.01$). Additionally, RRS1 exhibits upregulation in breast cancer ($p<0.001$), which is tightly linked to the occurrence of lymph node metastasis ($p<0.001$). Clinical breast cancer tissues and breast cancer cell lines also demonstrated a noteworthy upregulation of RRS1 ($p<0.05$). Loss-of-function experiment illustrated that the inhibiting of RRS1 expression reduced the rapid proliferation capacity of MDA-MB-231 and BT549 cells and hindered their migration and invasion capabilities ($p<0.05$). Importantly, the suppression of RRS1 significantly diminished lung metastasis in Balb/c nude mice that were injected with MDA-MB-231 cells ($p<0.01$). Mechanistically, RRS1 may interact with the AEG-1 to modulate the phosphorylation of AKT at T308 and S473, consequently impeding the activity of c-Myc ($p<0.05$). To conclude, RRS1 functions as a potential oncogene in breast cancer by leveraging the AEG-1/AKT/c-Myc signaling.

Key words: RRS1; AEG-1; breast cancer; migration and invasion

Breast cancer (BC) is the most widespread tumor in women globally [1]. Even though early diagnosis and standardized treatment have enhanced the 5-year patient survival rate to 90%, there is still a considerable number of deaths linked to BC recurrence and metastasis [2, 3]. The common subtypes of BC are luminal A, luminal B, Her-2 positive, and triple-negative BC (TNBC). TNBC lacks suitable therapeutic targets [4] and is easy to relapse and metastasize, resulting in non-responsive patients and an annual survival rate of merely 38.8% [5]. BC recurrence and metastasis are the main reasons for death [6, 7]. Consequently, an immediate search for novel genes associated with the migration and invasion of BC, and the identification of molecular mechanisms is imperative. These objectives aim to provide potential diagnostic markers and therapeutic targets, ultimately improving the survival and prognosis of BC patients.

Japanese researchers discovered RRS1 in yeast back in 2000 [8]. RRS1 plays a role in the maturation of *25S* rRNA

and the assembly and movement of *60S* ribosomal subunits within cells [9, 10]. Through the utilization of the high-content functional screening (HCS) platform, our previous study identified RRS1 as a crucial regulator of BC cell proliferation [11]. In recent years, RRS1 has been associated with cancer, specifically colorectal cancer, thyroid cancer, liver cancer, as well as BC. These tumors exhibited overexpression of RRS1. Cao *et al.* [12] found that RRS1 contributed to the malignant activity of hepatocellular carcinoma by disrupting the RPL11-MDM2-p53 signaling pathway. By reducing the RRS1 presence, the p53 pathway was upregulated, leading to the downregulation of cell cycle-related proteins (e.g., BRCA1, CDK1, and CCNB1) and the upregulation of cell cycle inhibitors (e.g., CDKN1A, FAS, and APP) in colorectal cancer. Ultimately, these alterations inhibited the proliferation of colon cancer cells [13]. Additionally, our previous report indicated abnormal overexpression of RRS1 in BC tissues, which further promoted excessive proliferation and metastasis of BC cells [14]. Nevertheless, the function and biomolecular mechanism of RRS1 in BC migration and invasion are not clear.

According to previous research, RRS1 was found to be highly expressed in brain tissue affected by Huntington's disease [15]. The researchers found that RRS1 was overexpressed in Huntington's disease and interacts with astrocyte elevatedgene-1 (AEG-1) to participate in endoplasmic reticulum stress responses, suggesting that RRS1 may promote the progression of Huntington's disease by interacting with AEG-1. AEG-1, a transmembrane protein, is unique to vertebrates and can be found in various cellular locations including the cytoplasm, endoplasmic reticulum, nuclear membrane, and nucleolus [16]. AEG-1 possesses dual functionalities, as it activates numerous oncogenes involved in tumor invasion, angiogenesis, metastasis, and resistance to chemicals. Simultaneously, it suppresses tumor suppressor genes, effectively preventing cell arrest and apoptosis while enhancing cell survival [17]. These effects are mainly achieved through the interaction of AEG-1 with various oncogenes such as PI3K, NF-κB, MMP-9, and Wnt [18–21]. Based on the findings mentioned above, it has been reported that AEG-1 plays a critical role in certain signaling pathways, potentially acting as a critical signaling molecule by binding to different substances within tumors. Hence, we aim to investigate whether RRS1 regulates the metastasis of BC through its association with AEG-1 and its downstream signaling pathway. This study strives to provide insights into the role of RRS1 in promoting BC metastasis, elucidate its molecular mechanism, and establish an experimental foundation for understanding the pathogenesis of BC metastasis.

Materials and methods

Bioinformatics analysis. Analyses were performed on 1,085 breast tumor samples and 291 normal breast tissues obtained from The Cancer Genome Atlas (TCGA) using the GEPIA shared database (http://gepia.cancer-pku.cn) to assess the discrepancies in RRS1 expression and survival curves in BC. Additionally, UALCAN datasets (https://ualcan.path.uab.edu/cgi-bin/ualcan-res.pl) were used to examine RRS1 expression levels in different BC subtypes and lymph node metastasis.

Ethics approval and consent to participate. This study was approved by the Ethics Committee of the Affiliated Hospital of Chengdu University of Traditional Chinese Medicine (approval ID: 2023KL-040) and performed in accordance with the tenets of the Declaration of Helsinki. All mouse experiments were performed in accordance with the ethical guidelines established by the Animal Ethics Committee of Qingdao University (approval number: No20200605).

Cell culture and lentivirus infection. Human BC cell lines MDA-MB-231, BT549, and MDA-MB-468 were obtained from Gene of China. Normal human mammary epithelial cells (HMECs) and BC cells MCF-7 were purchased from Gennio Biological Technology Company. All cells were cultured in high-glucose Dulbecco's Modified Eagle Medium (DMEM) supplemented with 10% fetal bovine serum (FBS) from Gibco, USA, and 100 μg/ml of penicillin/streptomycin. The cells were cultured at 37 °C in a humidified atmosphere with 5% CO_2. Lentiviral vectors were used to effectively integrate foreign shRNAs into host chromosomes to construct MDA-MB-231 and BT549 cell lines with RRS1 knockdown and for *in vivo* animal study the LUC-labeled-lentiviruses were applied (Supplementary Figures S2A, S2B). To introduce lentiviruses, MDA-MB-231 and BT549 cells were harvested and seeded in a 6-well plate. Upon the cell density reached 20–30%, the cells were transfected with either negative control lentiviruses or specific lentiviruses targeting RRS1 using HiTransG A and HiTransG P from Gene of China following the manufacturer's instructions. To calculate the viral load, we used the formula (Multiplicity of Infection × number of cells in mesh)/virus titer. All cell lines were mycoplasma-free (Vazyme Mycoplasma Detection Kit). All cell lines were authenticated shortly before the use by the STR technique, carried out by Gene of China.

RNA isolation and quantitative real-time PCR. The RNA was isolated from homogenized tissues and treated cells utilized the RNeasy isolation kit (Vazyme Biotech Co. Ltd., Nanjing, China). Afterward, reverse transcription was conducted using the Evo M-MLV RT kit with gDNA Clean for qPCR II (Accurate Biology, China) on Applied Biosystems (Thermo Fisher, USA). The cDNA amplification was performed using the SYBR green fuel method (Accurate Biology, Hunan, China) on a real-time fluorescence quantitative PCR instrument manufactured by Analytik Jena (Germany). For calculating the relative expression levels, the $2^{-\Delta\Delta ct}$ method was employed, using the human GAPDH gene as the internal control. The primers utilized in this study were outlined *GAPDH* F: 5'-AGAAGGCTGGGGCTCATTTG-3', R: 5'-AGGGGCCATCCACAGTCTTC-3'; *RRS1* F: 5'-CCCTACCGGACACCAGAGTAA-3', R: 5'-CC-

GAAAAGGGGTTGAAACTTCC-3'; *AEG-1* F: 5'-CGAGAAGCCCAAACCAAATG-3', R: 5'-TGGTGGCTGCTTTGCTGTT-3' and were synthesized by Gene of China.

Western blot. The cells undergoing treatment were lysed in RIPA buffer with the addition of protease and phosphatase excitation inhibitors for a duration of 30 min on ice. Subsequently, centrifugation was performed at 10,000 × g for 20 min. The protein concentration was detected by the BCA kit (Beyotime, China). Equal amounts of protein samples were run on an SDS-PAGE gel and transferred onto a PVDF membrane. After blocking with 5% BSA in TBST for 2 h at room temperature, the membranes were then incubated overnight with specific primary antibodies targeting various proteins, namely GAPDH (10494-1-AP; Proteintech), RRS1 (ab188161; Abcam), AEG-1 (ab227981; Abcam), AKT (60203-3-lg; Proteintech), phospho-AKT1 Thr308 (AF0832; Affinity Biosciences), phospho-AKT1 Ser473 (AF8355; Affinity Biosciences), c-Myc (#18583, Cell Signaling Technology). All antibodies were used at 1:1,000 dilution. Mouse and rabbit secondary antibodies were purchased from Proteintech (Cat No. SA00001-1/Cat No. SA00001-2) and incubated according to the manufacturer's instructions. Protein bands were assessed by means of enhanced chemiluminescence. The membranes were captured by the BIO-RAD Gel Doc™ XR+Imaging System (Bio-Rad, USA).

CCK-8 assay. Cells in the logarithmic growth phase were seeded on a 96-well plate at a density of 3×10^3 cells/well. Cell viability was measured daily from 0 to 5 d after transduction. After adding of 10 μl CCK-8 reagent (Yeasen Biotech Co., Ltd.) to each well, the cells were incubated for 1 h. The absorbance at 450 nm was determined using a microplate reader. Each experiment was triplicated.

Wound scratch assay. When the transfected cells reached 100% confluency, the cell monolayer was scratched with a sterile 200 μl pipette tip to imitate the wound area, and the wells were rinsed with medium to remove debris. Serum-free medium was added to continue culturing the cells for 24 h. The wound area was photographed at 0, 6, 12, and 24 h post-scratching, and the cell migration rate (%) was calculated as the percentage of wound area covered by the migrating cells to the total wound area.

Transwell migration and invasion assays. A density of 30,000 cells/well was allocated to the treated cells in the upper space of the Transwell inserts. These inserts, coated with or without Matrigel, were used while the lower space was filled with 600 μl of a complete medium containing 30% FBS. The samples were then cultivated for a duration of 24 to 48 h. Following this incubation period, the inserts were taken out and the cells remaining on the filter surface were gently swabbed. Transwell chambers and Matrigel were obtained from Corning (Corning, USA). To visualize cells migrating or invading the other side of the filter, they were fixed with 4% paraformaldehyde, stained with crystal violet (Sigma C3886; comprising 0.1% crystal violet in 20% methanol), and subsequently counted using a microscope.

Apoptosis evaluation. Flow cytometry was used to analyze cell apoptosis. After 48 h of transduction, cells were collected and washed twice with pre-cold PBS. Subsequently, the cells were re-suspended in 100 μl of binding buffer. Then, 2.5 μl Annexin-V-FITC and 2.5 μl PI (propidium iodide) were added to each sample and incubated at room temperature without light for 20 min according to the instructions of the Annexin V-FITC/PI Apoptosis Kit (Elabscience Biotechnology, China), binding buffer 400 μl was added before detection. The cells were then immediately evaluated using a flow cytometer (FACSCallibur, BD, USA). FlowJoTM version 10 software analyzed the data.

Analysis of cell cycle progression. The transfected cells were cleansed with PBS, digested, and harvested. Subsequently, the cells were fixed with 500 μl of 70% ethanol (volume fraction) for over 2 h at 4 °C. They were then rinsed twice with PBS at 500 × g for 3 min to eliminate ethanol. Each sample was treated with a cell cycle staining solution (RNase A:PI=1:9) of 500 μl following the guidelines of the Cell Cycle Detection Kit (KeyGEN BioTECH, China). The samples were shielded from light and incubated at room temperature for 30–60 min, while recording the red fluorescence at an excitation wavelength of 488 nm. The testing equipment and data analysis software used can be found in the Materials and methods 'Apoptosis evaluation' section.

Co-immunoprecipitation assay (Co-IP). The treated cells were lysed at 4 °C for 30 min. The lysates were incubated with 10 μl homologous IgG for 1 h, and then with an anti-AEG-1 antibody (1:200) overnight. Then the A/G Sepharose (Bio Linkedin, China) was added, and the lysates were incubated at 4 °C with constant agitation for 2 h. The immunoprecipitants were separated by SDS-PAGE after washing with the same buffer and analyzed by immunoblotting as described in the section western blot.

Establishment of *in vivo* tumor models. In summary, 10 Balb/c nude female mice, aged 3–4 weeks, were obtained from Beijing Vital River Laboratory Animal Technology Co. Ltd. They were then adaptively fed for one week in a specific pathogen-free environment. Luc-labeled lentiviral constructs expressing control shRNA (Luc-sh-Con) and RRS1 shRNA (Luc-sh-RRS1) were transfected into MDA-MB-231 cells. To induce tumor metastasis, 1×10^6 LUC-labeled cells were injected into the circulating blood of Balb/C nude mice via the tail vein (n=5). An *in vivo* imaging system (IVIS Spectrum, Perkin Elmer, USA) was employed to visualize the fluorescence intensity and specific location of the tumor cells in mice. The mice were anesthetized with isoflurane (VETEASY, China), using 3–4% for induction and 1–2% for maintenance. Additionally, the fluorescent enzyme substrate used was D-Luciferin, Potassium Salt D at a dosage of 150 mg/kg (i.p.) (Yeasen BioTechnologies, China). The observation time points were on day 1 and day 45. After the observation period had ended, the mice were euthanized humanely, and imaging was conducted on the major organs (heart, lung, liver, kidney, spleen) and bones. Picric acid staining was performed to

examine any surface nodules present on the lung tissue. Throughout a period of 45 d, the mice were closely monitored.

Hematoxylin-eosin staining. The detection of lung pathological changes in paraffin-embedded lung tissue sections was conducted using Bouin's fixative and H&E staining. Initially, 5 μm thick tissue sections were deparaffinized and rehydrated. Subsequently, these sections were subjected to a 5 min staining period using a hematoxylin solution. Following this, they underwent five washes using 1% acid ethanol (1% HCl in 70% ethanol) and were then saturated in deionized water. To complete the staining process, the sections were stained for 3 min using an eosin solution. The next steps involved dehydration through an ethanol gradient and clearance in xylene. Finally, the prepared slides were mounted and examined using an Olympus fluorescence microscope located in Tokyo, Japan.

Picric acid staining. Metastatic nodules were observed by picric acid staining. 24 h after the lung tissue of nude mice was fixed with a picric acid-saturated aqueous solution (1.22%, SBH.Bio), the lung tissue was removed to absorb excess water with absorbent paper, and the white nodules were observed with photos.

Statistical analysis. Mean ± standard error of the mean (SEM) was used to present all data, which were obtained from a minimum of three independent replicates. The statistical analysis was conducted utilizing GraphPad Prism software (version 9.0.0; GraphPad Inc., USA). To compare the distinction between the two groups, Student's t-test was utilized, while one-way ANOVA was performed to compare multiple groups.

Results

Biological function of RRS1 in BC. In order to find out the biological function of RRS1 in BC, we conducted an analysis of publicly available data. It revealed that RRS1 exhibited elevated expression levels in BC (Figure 1A, $p<0.001$), thereby indicating a detrimental prognosis for BC (Figure 1B, $p<0.05$). Analyses conducted on data from TCGA revealed that the expression levels of RRS1 were most pronounced in TNBC (Figure 1C, $p<0.001$) and exhibited a correlation with lymph node metastasis (Figure 1D, $p<0.001$). These findings collectively propose a potential association between heightened RRS1 expression and the progression and development of BC. To validate this hypothesis, we also investigated RRS1 mRNA overexpression in 25 sets of BC tissues and their corresponding adjacent normal tissues (Figure 1E, $p<0.05$). Similarly, RRS1 mRNA exhibited significant upregulation in BC cell lines (BT549, MDA-MB-231, MDA-MB-468) in comparison to normal HMECs (Figure 1F, $p<0.01$). Another noticeable observation was the consistent upregulation of RRS1 protein expression levels (Figure 1G, $p<0.001$). Hence, we postulate that the aberrant RRS1 expression in BC might be potentially associated with the onset and malignant activity of this highly invasive subtype.

Inhibition of BC cells proliferation *in vitro* by RRS1 knockdown. To investigate the contribution of RRS1 in BC, we conducted experiments involving the transduction of MDA-MB-231 (Supplementary Figure S1A) and BT549 cells (Supplementary Figure S1B) with EGFP-sh-CON and EGFP-sh-RRS1 lentiviruses, both groups exhibited about 70% transduction efficiency. Expectably, the sh-RRS1 group displayed a significant reduction in mRNA levels (Supplementary Figure S1C, $p<0.001$; Supplementary Figure S1D, $p<0.001$) and protein levels (Supplementary Figure S1E, $p<0.001$; Supplementary Figure S1F, $p<0.001$) compared to the sh-CON group. Additionally, RRS1 knockdown led to a decrease in the proliferation of MDA-MB-231 and BT549 cells, as demonstrated in Figures 2A and 2B ($p<0.05$). To investigate the impact of RRS1 knockdown on BC cells proliferation, we conducted apoptosis and cell cycle experiments. The findings revealed that RRS1 knockdown led to a statistically significant increase in apoptotic rates in MDA-MB-231 (Figure 2C, $p<0.01$) and BT549 cells (Figure 2D, $p<0.001$). Additionally, following RRS1 knockdown, the cell cycle progression of MDA-MB-231 (Figure 2E, $p<0.05$) and BT549 (Figure 2F, $p<0.001$) cells was significantly impeded in the S phase. In summary, downregulation of RRS1 likely induces the S phase arrest in BC cells, thereby suppressing proliferation and facilitating apoptosis.

RRS1 knockdown inhibited BC cells migration and invasion ability *in vitro*. To delve deeper into the contribution of RRS1 in the malignant behavior of BC, we conducted scratch wound healing assays and Transwell experiments (including those with and without Matrigel). The sh-RRS1 group exhibited significantly diminished wound healing rates (Figure 3A, $p<0.05$; Figure 3B, $p<0.05$), mobility (Figure 3C, $p<0.001$; Figure 3D, $p<0.01$), and invasiveness (Figure 3E, $p<0.001$; Figure 3F, $p<0.05$) compared to the sh-CON group. These findings elucidate that RRS1 knockdown leads to a substantial decline in the migration and invasion abilities of BC cells.

Knocking down of RRS1 inhibited BC cells metastasis *in vivo*. The promotion of migration and invasion of BC cells by RRS1 *in vitro* suggests its potential to influence BC metastasis *in vivo*. To validate this hypothesis, a metastasis model of BC was established in Balb/C nude mice (n=5) by intravenous injection of MDA-MB-231 cells transfected with luciferase-tagged sh-RRS1 (RRS1 knockdown) or sh-CON (negative control) lentiviruses. The decreased expression levels of RRS1 mRNA (Figure 4A, $p<0.001$) and protein (Figures 4B, 4C, $p<0.05$) were confirmed in the sh-RRS1 versus sh-CON cells. Live imaging of the mice immediately after injection showed that the luminescence was mainly concentrated in the tail vein and buttocks (Figure 4D), and there was no significant difference between the luminescence intensities of the sh-CON and sh-RRS1 groups (Figure 4D, $p > 0.05$). Forty-five days later, sh-CON cells primarily accumulated in the lungs, indicative of lung metastasis, whereas sh-RRS1 cells showed no significant metastasis *in vivo* (Figure 4E).

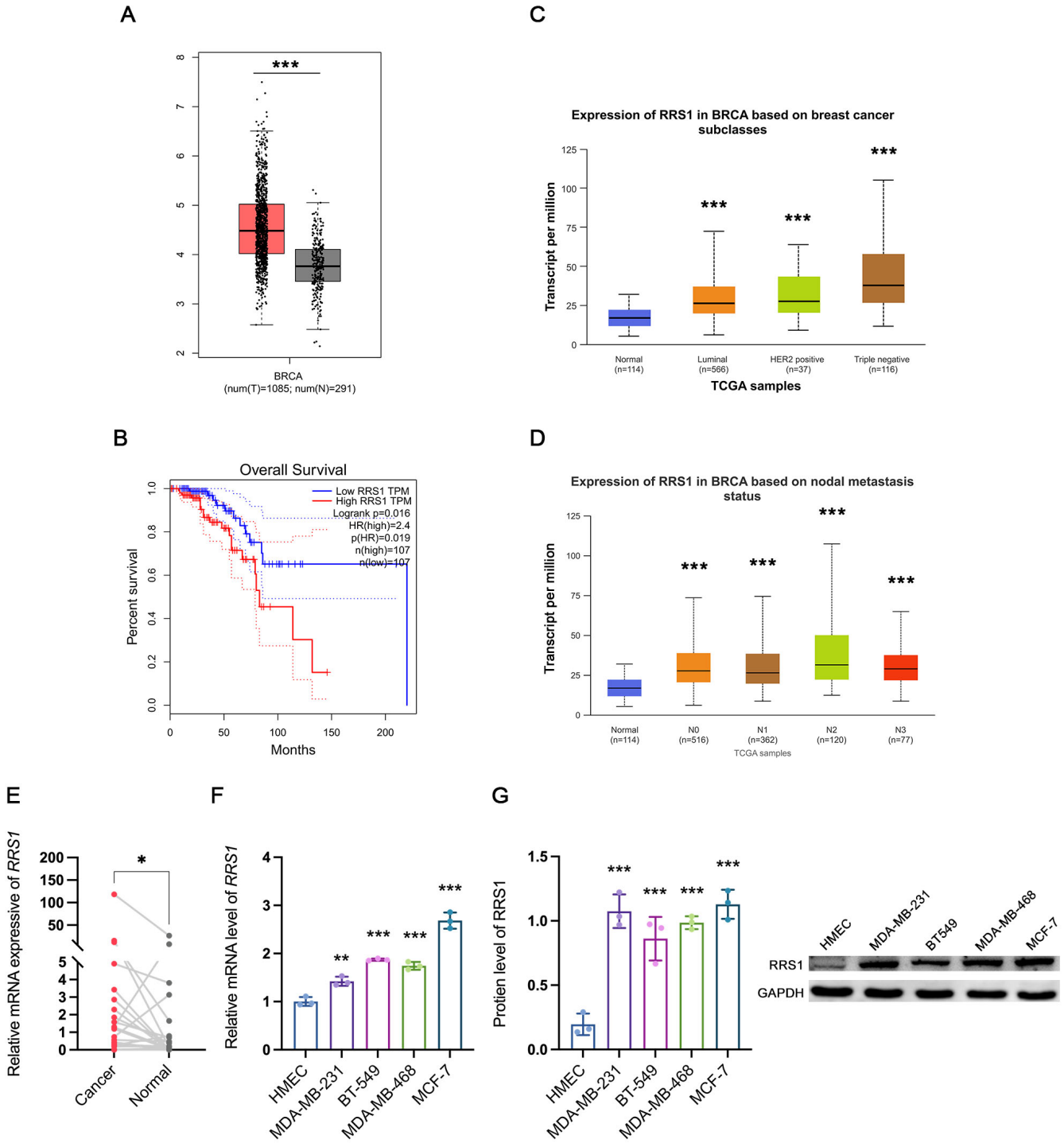

Figure 1. Expression of RRS1 in BC. A) Gene expression level of RRS1 in TCGA BC and matched TCGA normal breast tissues. BRCA stands for breast cancer. B) Kaplan-Meier survival analysis showed the correlation of RRS1 expression (Low, n=107 and High, n=107) of BC patients. C) RRS1 was most significantly upregulated in TNBC. D) The high expression of RRS1 in TNBC was associated with lymph node metastasis. E) RRS1 mRNA levels in 25 pairs of BC tissues and adjacent normal breast tissues detected by qRT-PCR. The mRNA (F) and protein (G) expression levels of RRS1 in HMEC cells and BC cell lines were determined by qRT-PCR and western blot. Notes: *p<0.05, **p<0.01, ***p<0.001 compared to the normal group, HMEC group, respectively; the Student's t-test analyzed the difference between the two groups, and one-way ANOVA compared the multiple groups

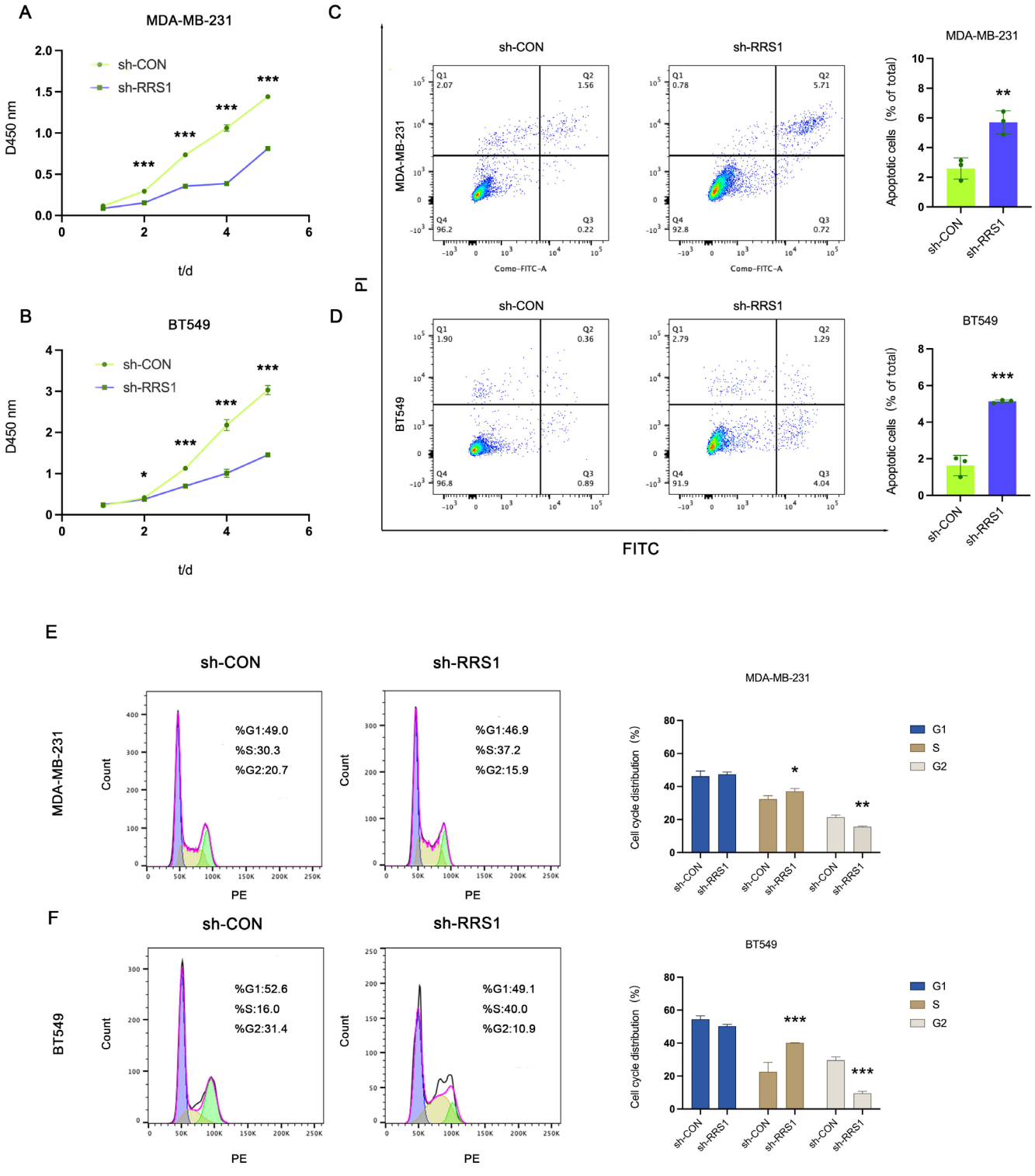

Figure 2. Effects of RRS1 knockdown on the proliferation and apoptosis of MDA-MB-231 cells and BT549 cells. A) MDA-MB-231 cells and B) BT549 cells proliferation capacities were assessed by the CCK-8 assay. C) MDA-MB-231 cells and D) BT549 cells apoptoses were detected by flow cytometry. Cell cycle distribution of E) MDA-MB-231 and F) BT549 cells were determined by PI staining following the transient RRS1 knockdown. Abbreviations: Sh-CON-Negative control; Sh-RRS1-RRS1 knockdown; Notes: *p<0.05, **p<0.01, ***p<0.001 compared to the sh-CON group; the Student's t-test analyzed the difference between the two groups

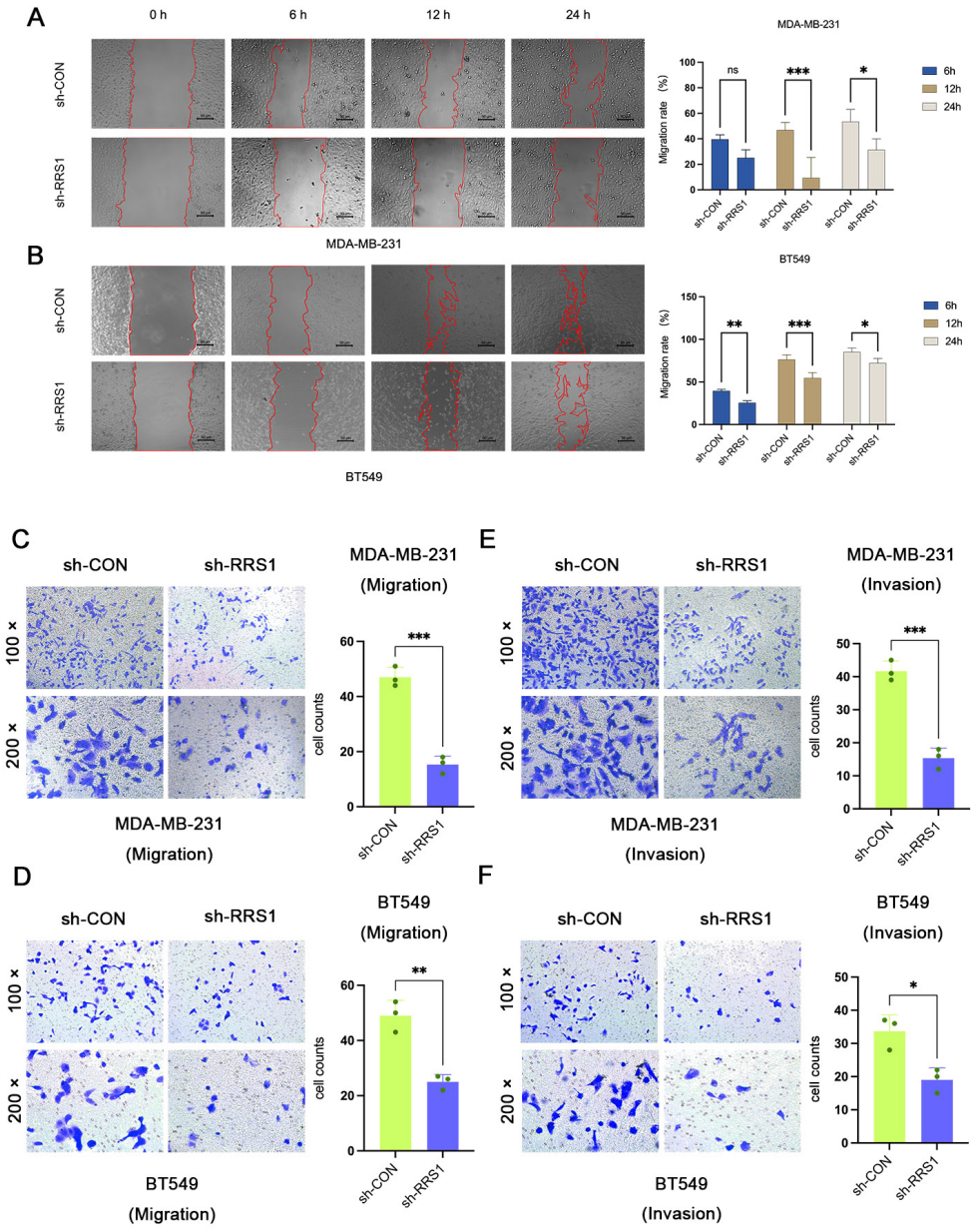

Figure 3. Effects of RRS1 knockdown on the migration and invasion of BC cells. A) Images of scratch wound healing assay and migration rates of MDA-MB-231 cells. B) Images of scratch wound healing assay and migration rates of BT549 cells. C) Images of migration Transwell assay without Matrigel and the number of invaded MDA-MB-231 cells. D) Images of migration Transwell assay without Matrigel and the number of invaded BT549 cells. E) Images of migration Transwell assay with Matrigel and the number of invaded MDA-MB-231 cells. F) Images of migration Transwell assay with Matrigel and the number of invaded BT549 cells. Abbreviations: Sh-CON-Negative control; Sh-RRS1-RRS1 knockdown; Notes: *p<0.05, **p<0.01, ***p<0.001 compared to the sh-CON group. The Student's t-test analyzed the difference between the two groups.

Moreover, the chemiluminescence intensity of the sh-CON group was impressively higher compared to the sh-RRS1 group (Figure 4E, p<0.01). Dissection of major organs (heart, liver, spleen, lungs, kidneys) and ex *vivo* imaging further supported metastases in the lungs of the sh-CON group, with reduced spread in the sh-RRS1 group (Figure 5A). The luminescence intensity was notably stronger in the sh-CON group (Figure 5B, p<0.001). Picrate staining demonstrated an increased number of nodules in the lungs of sh-CON mice as compared to the sh-RRS1 group (Figure 5C). H&E staining of lung tissue revealed solid lesions exclusively in the sh-CON group (Figure 5D). Thus, this study establishes the significant inhibition of BC lung metastasis *in vivo* upon RRS1 knockdown. In conclusion, this study demonstrated

that RRS1 knockdown significantly inhibited BC lung metastasis *in vivo*.

RRS1 knockdown inhibits the BC cells proliferation and metastasis through the AEG-1/AKT/c-Myc signaling pathway. Investigating the molecular mechanisms underlying the regulation of BC cells migration and invasion, the role of RRS1 has gained attention. Existing studies have highlighted the interaction between RRS1 and AEG-1 protein, suggesting a link between RRS1 and the development of Huntington's disease and tumor multidrug resistance[1]. Hence, we aimed to explore whether the regulation of AEG-1-mediated tumor promotion by RRS1 contributes to

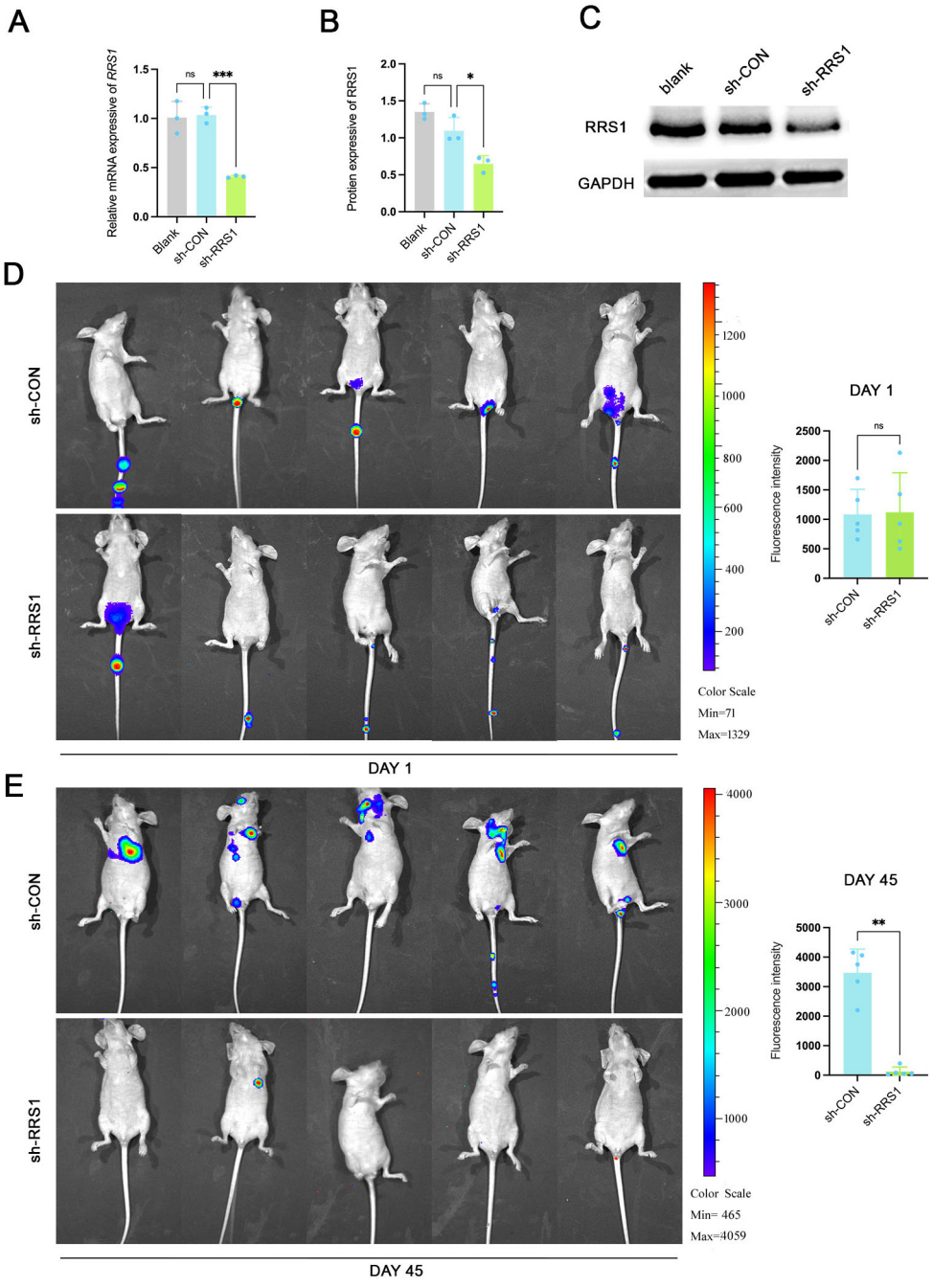

Figure 4. RRS1 knockdown significantly inhibited BC lung metastasis *in vivo*. A) RRS1 mRNA expression in the indicated cells. B, C) Immunoblot showing RRS1 protein levels in the indicated cells. Cell localization and chemiluminescence intensity *in vivo* in the murine metastasis model on D) day 1 and E) day 45. Abbreviations: Blank-untreated group; Sh-CON-Negative control; Sh-RRS1-RRS1 knockdown group; Notes: *p<0.05, **p<0.01, ***p<0.001 compared to the sh-CON group; the Student's t-test analyzed the difference between the two groups, and one-way ANOVA compared the multiple groups

BC metastasis. To investigate this, we examined the impact of RRS1 knockdown in MDA-MB-231 cells on the expression of AEG-1 and its downstream key proteins. The results showed that knockdown of RRS1 (Figures 6A, 6C, $p<0.05$) significantly decreased the expression of the AEG-1 protein (Figures 6A, 6D, $p<0.01$). Additionally, Co-IP assays uncovered a direct physical interaction between RRS1 and AEG-1 in BC cells (Figure 6B). In tumor cells, the AEG-1 protein activates the AKT pathway through phosphorylation, thereby modulating proliferation and migration. Consequently, we assessed the expression levels of total AKT, phosphorylated AKT, and its downstream protein c-Myc. The results showed that the total expression amount of AKT did not change (Figures 6A, 6E, $p>0.05$), but P-AKT^{T308} (Figures 6A, 6F, $p<0.001$) and P-AKT^{S473} (Figures 6A, 6G, $p<0.05$) showed significant inhibition suppressing the nuclear translocation of c-Myc expression (Figures 6A, 6H, $p<0.05$). In summary, these findings demonstrate that RRS1 knockdown inhibits BC proliferation and metastasis, likely via the AEG-1/AKT/c-Myc signaling axis.

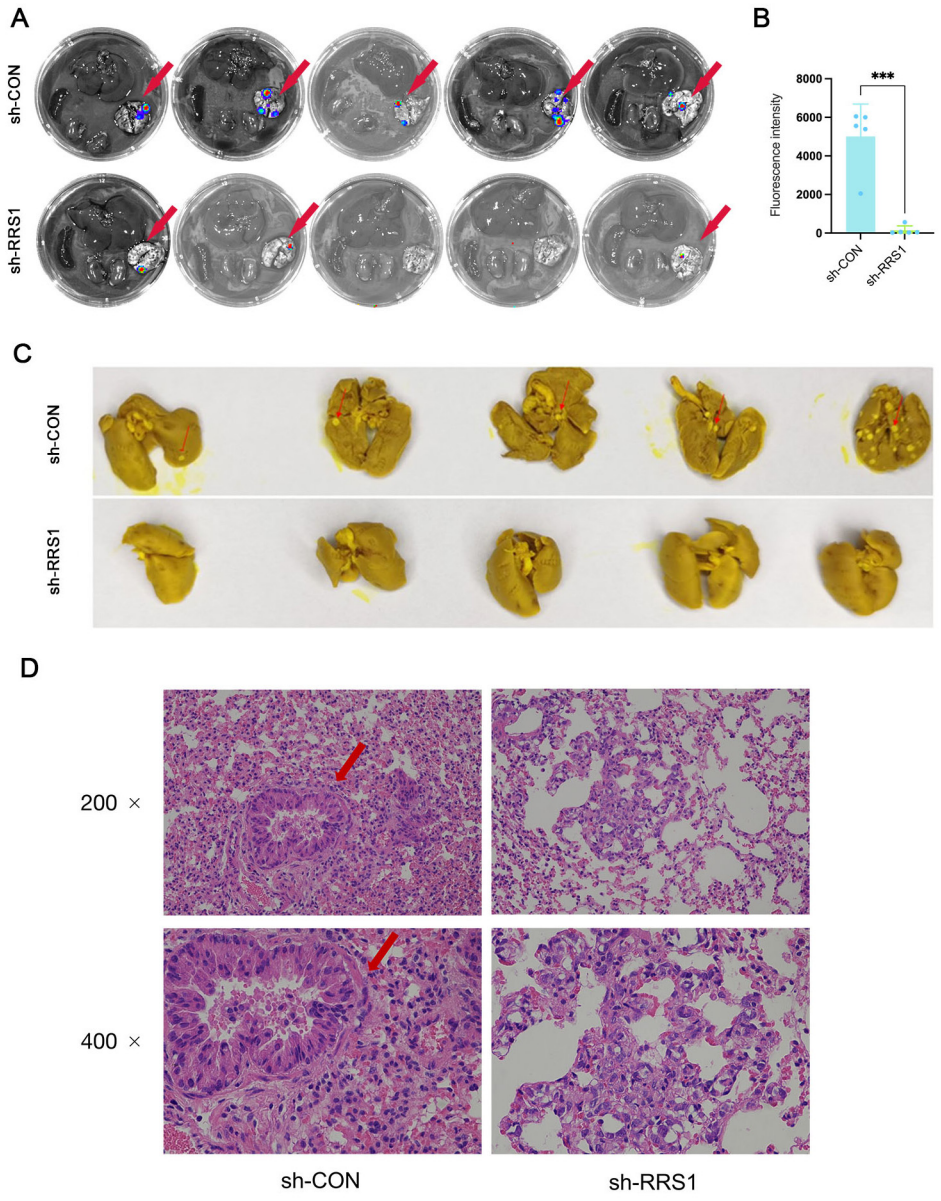

Figure 5. BC lung metastases in nude mice. A) *Ex vivo* imaging of heart, liver, spleen, lungs, and kidneys, red arrows indicated fluorescent lungs. B) The lung chemiluminescence intensity of the sh-CON and sh-RRS1 groups. C) Representative images of picric acid staining and D) H&E-stained of lung tissues of the sh-CON and sh-RRS1 groups, the samples were imaged at ×200 and ×400, red arrows indicated pulmonary nodules and metastases. Abbreviations: Sh-CON-Negative control; Sh-RRS1-RRS1 knockdown group); Notes: *p<0.05, **p<0.01, ***p<0.001 compared to the sh-CON group; the Student's t-test analyzed the difference between the two groups

Discussion

According to the data released in 2021, BC has surpassed lung cancer as the most prevalent form of cancer, with an incidence rate of 11.7%. It is also the most frequently diagnosed tumor in women, accounting for 24.5% of cases [22, 23]. Despite advancements in diagnostic and therapeutic strategies, the 5-year survival rates for BC patients remain low due to the high occurrence of either recurrence or metastasis. The metastasis of BC is a complex process involving multiple mechanisms, and the precise molecular mechanisms behind it are still unclear. Our research reveals that RRS1 plays a crucial biotic factor in promoting the invasion and migration of BC cells through the AEG-1/AKT/c-Myc signaling pathway.

RRS1 is a protein involved in ribosome biosynthesis and has recently been identified as an oncogene. A study conducted by He *et al.* using the integrative omics analysis demonstrated that RRS1 is implicated in the initiation and progression of liver cancer [12]. Additionally, RRS1 has been found to be overexpressed in neuroblastoma [24]. In a previous investigation, we examined 242 breast tumor samples and detected RRS1 expression in 60.7% of them. Among these samples, 50% exhibited high levels of RRS1 expression [11]. Our study also noted high mRNA expression of RRS1 in breast tumor samples. Moreover, BC cell lines demonstrated significantly elevated levels of RRS1 compared to normal HMECs. Another study indicated that the upregulation of RRS1 in cells promotes their invasive behavior [25]. Aligning with these findings, our study demonstrated that knocking down RRS1 in two BC cell lines suppressed their invasion and migration *in vitro*. These results suggest that RRS1 presents itself as a promising target for regulating metastasis in multiple types of tumors. Furthermore, our experiments using RRS1-knockdown MDA-MB-231 cells showed significantly reduced metastasis in immunodeficient mice compared to untreated MDA-MB-231 cells. Hence, RRS1 acts as an oncogene, facilitating the invasion and migration of BC cells.

AEG-1 is abnormally expressed in different types of tumors and enhances tumor proliferation, and AEG-1 often interacts with other proteins to form protein complexes and exert its effects. It is also reported in Huntington's disease that RRS1 interacts with AEG-1 to promote disease progression, so we propose the hypothesis that RRS1 interacts with AEG-1 to inhibit its expression and prevent BC cell migration and invasion. Accordingly, we centered on and executed a Co-IP experiment to affirm the interaction between RRS1 and AEG-1. Aligning with this, we discovered that the downregulation of RRS1 also diminished AEG-1 levels, and Co-IP revealed a direct physical binding between the two proteins. These findings propose that RRS1 might bind to and boost the levels of AEG-1 in BC cells, which could be the underlying mechanism for its oncogenic effects. Our outcomes are in line with prior investigations. Suppression of AEG-1 resulted in a decline in the phosphorylation levels

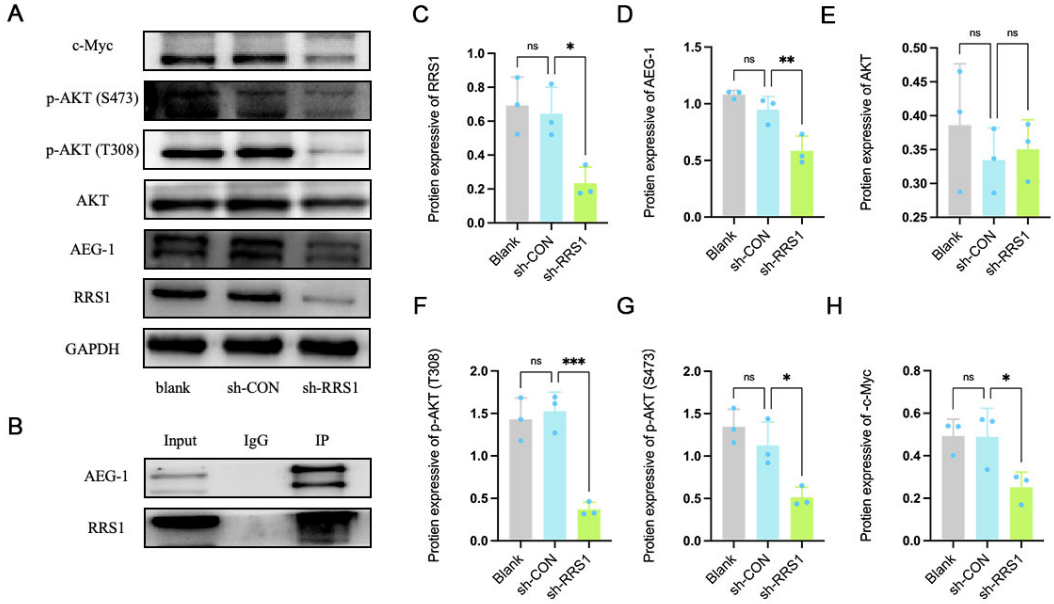

Figure 6. RRS1 knockdown inhibits the BC cells malignant activity through the AEG-1/AKT/c-Myc signaling. A) Representative western blot images of MDA-MB-231 cells. B) Co-IP experiment of RRS1 and AEG-1. C) RRS1 protein levels in MDA-MB-231 cells after RRS1 knockdown. Quantification of D) AEG-1, E) AKT, F) p-AKT (T308)/AKT, G) p-AKT (S473)/AKT, and H) c-Myc. Abbreviations: Blank-Untreated group; Sh-CON-Negative control; Sh-RRS1-RRS1 knockdown group; Notes: *p<0.05, **p<0.01, ***p<0.001 compared to the sh-CON group; One-way ANOVA compared the multiple groups

of AKT and a subsequent reduction in the expression of the c-Myc protein associated with metastasis. This led to a reduction in invasion and migration of BC cells.

The complex regulatory process of BC migration and invasion involves various mechanisms. These mechanisms include the initiation of the EMT process, activation of the AKT and c-Myc signaling pathway, remodeling of the microenvironment in the sentinel lymph nodes, and metabolic irregularities in tumor cells [26–29]. Our research focuses on investigating the role of RRS1 in promoting the migration and invasion of BC cells. It is suggested that this promotion occurs through the AEG-1/AKT/c-Myc signaling pathway. In our study, we not only observed the *in vitro* regulation of invasion and migration abilities of MDA-MB-231 and BT549 cells by RRS1 but also identified its potential role in regulating lung metastasis of BC cells *in vivo* for the first time. These findings provide valuable laboratory data for identifying potential metastatic targets for breast cancer. However, further studies are needed to gain a deeper understanding of the mechanisms underlying RRS1 and AEG-1 regulation of migration and invasion in BC cells. Additionally, we have explored the related molecular mechanisms of RRS1's function, which provide more evidence for the role of RRS1 in the progression of BC. In our *in vivo* experiments, we used the method of injecting tumor cells into the tail vein for modeling, but *in situ* tumors may have more guiding significance for the study of metastasis. In future experiments, we will further use *in situ* tumor models for research. For the function of RRS1 in BC metastasis, we also need to explore the mechanism more deeply.

In conclusion, our investigation has uncovered the crucial role of RRS1 in promoting BC progression by enhancing tumor cell apoptosis, migration, and invasion. These effects are believed to be mediated through the activation of the AEG-1/AKT/c-Myc pathway. These findings contribute to a better understanding of the mechanisms by which BC develops and provide important insights into potential therapeutic targets for BC.

Supplementary information is available in the online version of the paper.

Acknowledgments: Thanks for the technical support of scholars from the Innovation Research Institute of Chengdu University of Traditional Chinese Medicine. This work was supported by the National Natural Science Foundation of China (No. 81872959, No. 81373920, No. 30801522) and the Natural Science Foundation of Sichuan Province (Grant no. 2022NSFSC0733).

References

[1] ARNOLD M, MORGAN E, RUMGAY H, MAFRA A, SINGH D et al. Current and future burden of breast cancer: Global statistics for 2020 and 2040. Breast 2022; 66: 15–23. https://doi.org/10.1016/j.breast.2022.08.010

[2] ABDERRAHMAN B, JORDAN VC. Telling details of breast-cancer recurrence. Nature 2018; 553: 155. https://doi.org/10.1038/d41586-018-00399-6

[3] GANESH K, MASSAGUÉ J. Targeting metastatic cancer. Nat Med 2021; 27: 34–44. https://doi.org/10.1038/s41591-020-01195-4

[4] DENKERT C, LIEDTKE C, TUTT A, VON MINCKWITZ G. Molecular alterations in triple-negative breast cancer-the road to new treatment strategies. Lancet 2017; 389: 2430–2442. https://doi.org/10.1016/s0140-6736(16)32454-0

[5] VAN UDEN DJP, VAN MAAREN MC, BULT P, STROBBE LJA VAN DER HOEVEN JJM et al. Pathologic complete response and overall survival in breast cancer subtypes in stage III inflammatory breast cancer. Breast Cancer Res Treat 2019; 176: 217–226. https://doi.org/10.1007/s10549-019-05219-7

[6] FOULKES WD, SMITH IE, REIS-FILHO JS. Triple-negative breast cancer. N Engl J Med 2010; 363: 1938–1948. https://doi.org/10.1056/NEJMra1001389

[7] CRIVELLI P, LEDDA RE, PARASCANDOLO N, FARA A, SORO D et al. A New Challenge for Radiologists: Radiomics in Breast Cancer. Biomed Res Int 2018; 2018: 6120703. https://doi.org/10.1155/2018/6120703

[8] TSUNO A, MIYOSHI K, TSUJII R, MIYAKAWA T, MIZUTA K. RRS1, a conserved essential gene, encodes a novel regulatory protein required for ribosome biogenesis in Saccharomyces cerevisiae. Mol Cell Biol 2000; 20: 2066–2074. https://doi.org/10.1128/mcb.20.6.2066-2074.2000

[9] NARIAI M, TANAKA T, OKADA T, SHIRAI C, HORIGOME C et al. Synergistic defect in 60S ribosomal subunit assembly caused by a mutation of Rrs1p, a ribosomal protein L11-binding protein, and 3'-extension of 5S rRNA in Saccharomyces cerevisiae. Nucleic Acids Res 2005; 33: 4553–4562. https://doi.org/10.1093/nar/gki772

[10] GAMBE AE, MATSUNAGA S, TAKATA H, ONO-MANIWA R, BABA A et al. A nucleolar protein RRS1 contributes to chromosome congression. FEBS Lett 2009; 583: 1951–1956. https://doi.org/10.1016/j.febslet.2009.05.033

[11] SONG J, MA Z, HUA Y, XU J, LI N et al. Functional role of RRS1 in breast cancer cell proliferation. J Cell Mol Med 2018; 22: 6304–6313. https://doi.org/10.1111/jcmm.13922

[12] CAO P, YANG A, LI P, XIA X, HAN Y et al. Genomic gain of RRS1 promotes hepatocellular carcinoma through reducing the RPL11-MDM2-p53 signaling. Sci Adv 2021; 7: eabf4304. https://doi.org/10.1126/sciadv.abf4304

[13] WU XL, YANG ZW, HE L, DONG PD, HOU MX et al. RRS1 silencing suppresses colorectal cancer cell proliferation and tumorigenesis by inhibiting G2/M progression and angiogenesis. Oncotarget 2017; 8: 82968–82980. https://doi.org/10.18632/oncotarget.20897

[14] WANG R, PENG C, SONG J, HUA Y, WU Q et al. Downregulated RRS1 inhibits invasion and metastasis of BT549 through RPL11 c Myc SNAIL axis. Int J Oncol 2022; 60: 33. https://doi.org/10.3892/ijo.2022.5323

[15] CARNEMOLLA A, FOSSALE E, AGOSTONI E, MICHELAZZI S, CALLIGARIS R et al. Rrs1 is involved in endoplasmic reticulum stress response in Huntington disease. J Biol Chem 2009; 284: 18167–18173. https://doi.org/10.1074/jbc.M109.018325

[16] SUTHERLAND HG, LAM YW, BRIERS S, LAMOND AI, BICKMORE WA. 3D3/lyric: a novel transmembrane protein of the endoplasmic reticulum and nuclear envelope, which is also present in the nucleolus. Exp Cell Res 2004; 294: 94–105. https://doi.org/10.1016/j.yexcr.2003.11.020

[17] OSAMA M, MOSTAFA MN, ALVI MA. Astrocyte elevated gene-1 as a novel therapeutic target in malignant gliomas and its interactions with oncogenes and tumor suppressor genes. Brain Res 2020; 1747: 147034. https://doi.org/10.1016/j.brainres.2020.147034

[18] XIE Y, ZHONG D. AEG-1 is associated with hypoxia-induced hepatocellular carcinoma chemoresistance via regulating PI3K/AKT/HIF-1alpha/MDR-1 pathway. EXCLI J 2016; 15: 745–757. https://doi.org/10.17179/excli2016-694

[19] YU X, WANG Y, QIU H, SONG H, FENG D et al. AEG-1 Contributes to Metastasis in Hypoxia-Related Ovarian Cancer by Modulating the HIF-1alpha/NF-kappaB/VEGF Pathway. Biomed Res Int 2018; 2018: 3145689. https://doi.org/10.1155/2018/3145689

[20] LIU X, LV Z, ZOU J, LIU X, MA J et al. Elevated AEG-1 expression in macrophages promotes hypopharyngeal cancer invasion through the STAT3-MMP-9 signaling pathway. Oncotarget 2016; 7: 77244–77256. https://doi.org/10.18632/oncotarget.12886

[21] LV S, ZHANG J, HE Y, LIU Q, WANG Z et al. MicroRNA-520e targets AEG-1 to suppress the proliferation and invasion of colorectal cancer cells through Wnt/GSK-3β/β-catenin signalling. Clin Exp Pharmacol Physiol 2020; 47: 158–167. https://doi.org/10.1111/1440-1681.13185

[22] SIEGEL RL, MILLER KD, FUCHS HE, JEMAL A. Cancer Statistics, 2021. CA Cancer J Clin 2021; 71: 7–33. https://doi.org/10.3322/caac.21654

[23] SUNG H, FERLAY J, SIEGEL RL, LAVERSANNE M, SOERJOMATARAM I et al. Global Cancer Statistics 2020: GLOBOCAN Estimates of Incidence and Mortality Worldwide for 36 Cancers in 185 Countries. CA Cancer J Clin 2021; 71: 209–249. https://doi.org/10.3322/caac.21660

[24] ZHANG X, LIU C, CAO Y, LIU L, SUN F et al. RRS1 knockdown inhibits the proliferation of neuroblastoma cell via PI3K/Akt/NF-κB pathway. Pediatr Res 2022. https://doi.org/10.1038/s41390-022-02073-0

[25] YAN X, WU S, LIU Q, ZHANG J. RRS1 Promotes Retinoblastoma Cell Proliferation and Invasion via Activating the AKT/mTOR Signaling Pathway. Biomed Res Int 2020; 2020: 2420437. https://doi.org/10.1155/2020/2420437

[26] FEDELE M, SGARRA R, BATTISTA S, CERCHIA L, MANFIOLETTI G. The Epithelial-Mesenchymal Transition at the Crossroads between Metabolism and Tumor Progression. Int J Mol Sci 2022; 23: 800. https://doi.org/10.3390/ijms23020800

[27] HINZ N, JÜCKER M. Distinct functions of AKT isoforms in breast cancer: a comprehensive review. Cell Commun Signal 2019; 17:154. https://doi.org/10.1186/s12964-019-0450-3

[28] GAO FY, LI XT, XU K, WANG RT, GUAN XX. c-MYC mediates the crosstalk between breast cancer cells and tumor microenvironment. Cell Commun Signal 2023; 21: 28. https://doi.org/10.1186/s12964-023-01043-1

[29] LI YL, HUNG WC. Reprogramming of sentinel lymph node microenvironment during tumor metastasis. J Biomed Sci 2022; 29: 84. https://doi.org/10.1186/s12929-022-00868-1

https://doi.org/10.4149/neo_2024_240122N35

The role of RRS1 in breast cancer cells metastasis and AEG-1/AKT/c-Myc signaling pathway

Jing HE[1,2,#], Sijing LIU[1,2,#], Shajie LUO[1,2], Jiaojiao FU[1,2], Zhengyue LIAO[1,2], Junying SONG[3], Jinlin GUO[1,2,*], Ya'nan HUA[1,2,3,*]

Supplementary Information

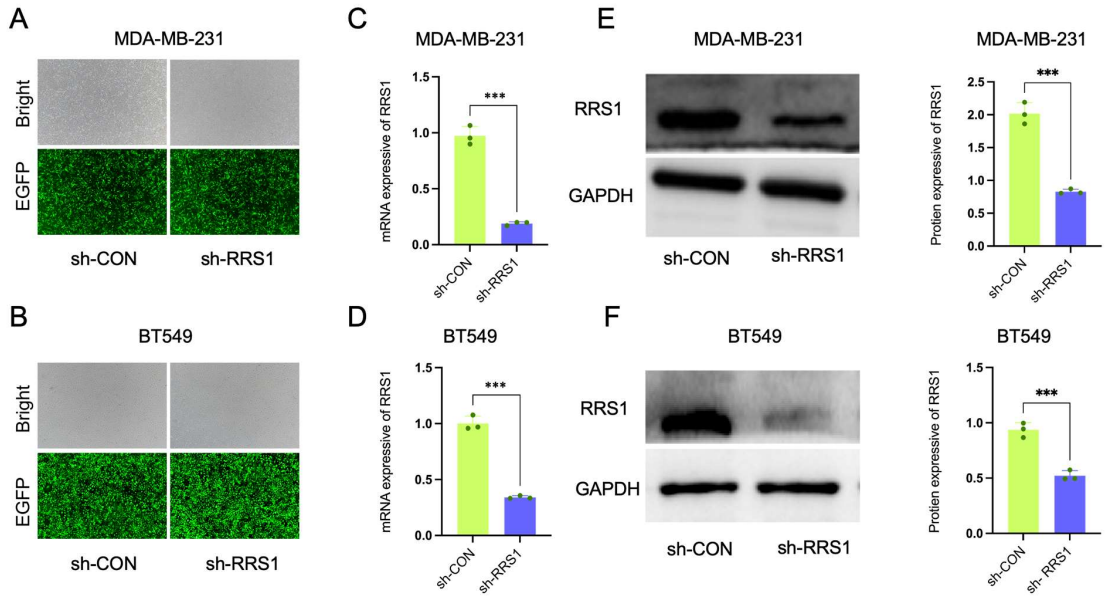

Supplementary Figure S1. For *in vitro* studies, EGFP stably transfected cell lines (sh-CON and sh-RRS1) were established. Fluorescence image of A) MDA-MB-231 cells and B) BT549 cells transfected with EGFP-labeled-lentiviral. The RRS1 mRNA expression of C) MDA-MB-231 cells and D) BT549 cells after transfected. E) Immunoblot showing RRS1 protein levels in the transfected of MDA-MB-231 cells and RRS1 protein expression. F) Immunoblot showing RRS1 protein levels in the transfected of BT549 cells and RRS1 protein expression. Sh-CON (Negative control); Sh-RRS1 (RRS1 knockdown). Notes: *p<0.05, **p<0.01; ***p<0.001 compared to the sh-CON group; the student's t-test analyzed the difference between the two groups.

A

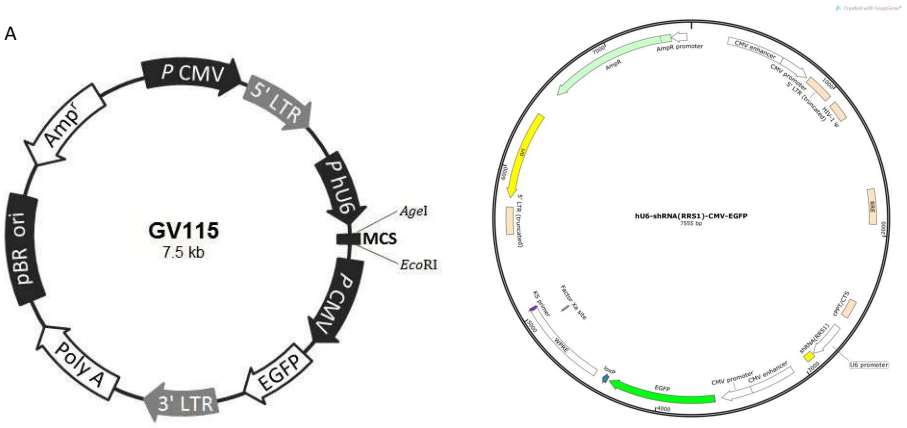

Targeting shRNA sequence: 5'GCTGCCTTCATTGAGTTTA3'

Negative control shRNA sequence: 5'TTCTCCGAACGTGTCACGT3'

B

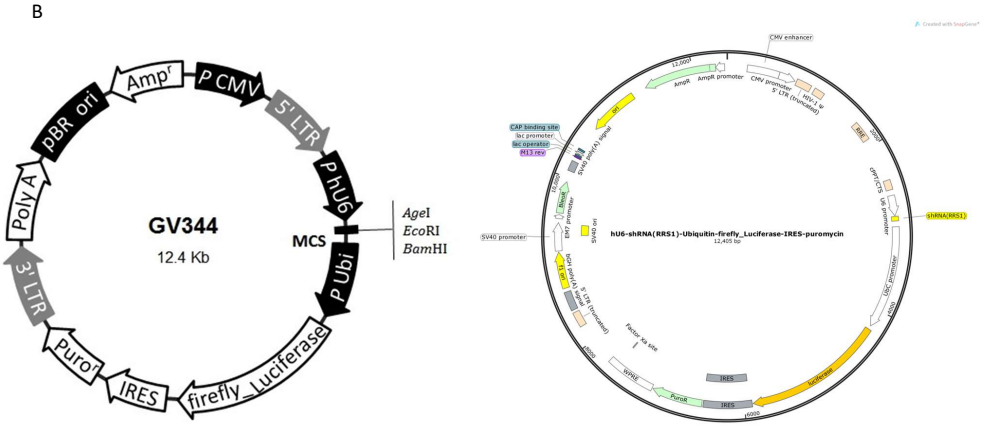

Targeting shRNA sequence: 5'GCTGCCTTCATTGAGTTTA3'

Negative control shRNA sequence: 5'TTCTCCGAACGTGTCACGT3'

Supplementary Figure S2. Details of lentiviral plasmids used to construct RRS1 knockdown breast cancer cell lines in cells and *in vivo* animal experiments. A) The lentiviral plasmids of EGFP-labeled-lentiviral, B) The LUC-labeled-lentiviral.